Received: 2 July 2019 | Revised: 26 November 2019 | Accepted: 27 November 2019

DOI: 10.1002/nbm.4242

RESEARCH ARTICLE

NMR IN BIOMEDICINE WILEY

Quantitative T1 mapping indicates tumor infiltration beyond the enhancing part of glioblastomas

Ulrike Nöth[1] | Julia Tichy[2] | Stephanie Tritt[3] | Oliver Bähr[2] | Ralf Deichmann[1] | Elke Hattingen[3]

[1]Brain Imaging Center, Goethe University, Frankfurt am Main, Germany

[2]Dr Senckenberg Institute of Neurooncology, Goethe University, Frankfurt am Main, Germany

[3]Institute of Neuroradiology, Goethe University, Frankfurt am Main, Germany

Correspondence
Ulrike Nöth, Goethe University, Brain Imaging Center (BIC), Schleusenweg 2-16, 60528 Frankfurt am Main, Germany.
Email: noeth@med.uni-frankfurt.de

The aim of this study was to evaluate whether maps of quantitative T1 (qT1) differences induced by a gadolinium-based contrast agent (CA) are better suited than conventional T1-weighted (T1w) MR images for detecting infiltration inside and beyond the peritumoral edema of glioblastomas. Conventional T1w images and qT1 maps were obtained before and after gadolinium-based CA administration in 33 patients with glioblastoma before therapy. The following data were calculated: (i) absolute qT1-difference maps (qT1 pre-CA - qT1 post-CA), (ii) relative qT1-difference maps, (iii) absolute and (iv) relative differences of conventional T1w images acquired pre- and post-CA. The values of these four datasets were compared in four different regions: (a) the enhancing tumor, (b) the peritumoral edema, (c) a 5 mm zone around the pathology (defined as the sum of regions a and b), and (d) the contralateral normal appearing brain tissue. Additionally, absolute qT1-difference maps (displayed with linear gray scaling) were visually compared with respective conventional difference images. The enhancing tumor was visible both in the difference of conventional pre- and post-CA T1w images and in the absolute qT1-difference maps, whereas only the latter showed elevated values in the peritumoral edema and in some cases even beyond. Mean absolute qT1-difference values were significantly higher ($P < 0.01$) in the enhancing tumor (838 ± 210 ms), the peritumoral edema (123 ± 74 ms) and in the 5 mm zone around the pathology (81 ± 31 ms) than in normal appearing tissue (32 ± 35 ms). In summary, absolute qT1-difference maps—in contrast to the difference of T1w images—of untreated glioblastomas appear to be able to visualize CA leakage, and thus might indicate tumor cell infiltration in the edema region and beyond. Therefore, the absolute qT1-difference maps are potentially useful for treatment planning.

KEYWORDS

gadolinium-based contrast agent, glioblastoma, infiltration, longitudinal relaxation time T1, quantitative MRI, quantitative T1-difference maps, edema

1 | INTRODUCTION

In MRI, signal enhancement after intravenous administration of a contrast agent (CA) is a hallmark of World Health Organization (WHO) grade IV glioblastomas.[1] The enhancement is the result of a deficient blood-tumor barrier of tumor-associated neovasculature that allows the CA to accumulate in the tumor tissue. Apart from the diagnostic value, identification of tumor regions enhancing after CA administration has implications for treatment. For example, the extent of resection of the enhancing part of a glioblastoma correlates with the survival time of the patients.[2-5] Unfortunately, conventional MRI tends to underestimate the extent of diffuse infiltrative glioma growth, as the infiltrating cells' spread exceeds the enhancing part of the tumor.[6,7] It is known that glioma cells migrate into the tumor edema, which appears hyperintense on T2-weighted (T2w) and FLAIR images, or even beyond.[8] Recurrent glioblastomas often arise from resection margins, suggesting that this area of recurrence represents the nonenhancing infiltration zone. Therefore, better knowledge of the nonenhancing infiltration areas would either allow their resection or their integration in the radiation field to prevent early tumor recurrences.

There is some evidence that metabolic imaging such as MR spectroscopic imaging (MRSI) and positron emission tomography (PET) using amino acid tracers, or diffusion tensor imaging (DTI), better depict the tumor cell infiltration near the enhancing areas than conventional MRI.[9-13] However, PET is an expensive method in addition to MRI and not always available, whereas DTI and especially MRSI have a limited spatial resolution and are prone to field inhomogeneity artifacts. Perfusion-weighted imaging assesses the cerebral blood volume (CBV) that correlates with both vascularization and tumor WHO grade.[14,15] Thus, increased CBV may also indirectly indicate infiltrating glioma cells if tumor infiltration is characterized by changes in vascularization.[16] In the diffuse infiltration zone, glioma cells first coopt preexisting vasculature, and once the tumor outgrows this supply, hypoxia may induce angiogenesis.[17,18] The vessel cooption and the first angiogenic trigger may impair the blood–brain barrier (BBB) and thus evoke subtle leakage of CA without increasing the CBV. Therefore, it is hypothesized that a method allowing for quantification of subtle CA accumulation might be able to detect infiltration of glioma cells outside of the strongly enhancing tumor area earlier than conventional MRI.

Due to their paramagnetic properties, gadolinium (Gd)-based CAs (GBCAs) shorten the relaxation times (T1, T2 and T2*), so that enhancing lesions appear hyperintense on contrast-enhanced T1-weighted (T1w) images and hypointense on quantitative T1 (qT1) maps post-CA. Therefore, the acquisition of qT1 maps before ($qT1_{pre}$) and after ($qT1_{post}$) intravenous GBCA administration allows for the calculation of qT1-difference maps, yielding an objective parameter for the assessment of even small amounts of GBCA accumulation. A potential drawback of this method is that patient movement can pose a problem for data subtraction. However, the advantage is that the qT1-difference maps are not merely assessed visually on the basis of image contrasts, but objectively on the basis of numerical T1 difference values. By contrast, the diagnostic quality of conventional T1w images post-CA ($T1w_{post}$) depends strongly on the hardware used and the choice of imaging parameters, and therefore to a greater extent on the visual capabilities and perception of the radiologist.

The purpose of the current study was to investigate the potential of qT1-difference maps in patients with glioblastomas before treatment. The aims were to (i) visually compare the absolute qT1-difference maps with the respective relative and absolute difference images of the conventional T1w images pre- and post-GBCA administration, and (ii) to quantify and compare absolute and relative GBCA-induced differences both of qT1 values and of signal intensities in T1w images. Comparison was performed for four volumes of interest (VOIs): (a) the enhancing tumor, (b) the adjacent nonenhancing edema with prolonged T2, (c) a 5 mm zone around the combined regions (a) and (b), and (d) normal appearing tissue in the contralateral hemisphere.

2 | MATERIALS AND METHODS

2.1 | Patients

The study was approved by the ethics committee of the University Hospital of the Goethe University Frankfurt am Main and written informed consent was obtained from all patients before participation.

The inclusion criteria for this study were: (i) suspected high-grade glioma based on conventional MRI, (ii) the glioma being accessible for stereotactic biopsy or tumor resection, (iii) the patient being able to give informed consent, and (iv) the patient being compliant for the MR study. Fifty-two patients (22 females, age range: 26 to 88 years, mean age ± SD: 62 ± 13 years) were enrolled. The MRI scans for this study were performed 1–3 days before surgery. Histopathology of tumor tissue resulted in the final diagnosis of high-grade glioma grade IV (glioblastoma) in 44 of these patients, of metastasis in two patients, of grade II meningioma in one patient, of astrocytoma grade II in one patient, and of astrocytoma grade III in three patients. In one patient no biopsy was performed. Only 33 of the 44 glioblastoma patients were included for further analysis as 11 had to be excluded for the following reasons: severe movement artifacts (four), qT1 scan before or after GBCA was not performed (three), and no coregistration between T1 and T2 maps was possible (two). Two further patients were excluded from the analysis: one patient did not have a peritumoral edema and the edema edge could not be defined in the other patient.

2.2 | Acquisition of MRI data

MRI data were acquired on a 3 T whole body scanner (Magnetom Verio, Siemens, Erlangen, Germany) using a body transmit and an eight-channel phased-array head receive coil.

For 3D qT1 mapping, the variable flip angle (VFA) technique[19] was employed, based on the acquisition of a proton density (PD)-weighted and a T1w spoiled gradient echo dataset by using two different excitation angles. Furthermore, the signal-to-noise ratio was improved by using a FLASH-EPI hybrid readout.[20] The imaging parameters were: FOV = 256 x 224 x 160 mm^3, matrix = 256 x 224 x 160, TR/TE/α_1/α_2 = 16.4 ms/6.7 ms/4°/24°, receiver bandwidth = 222 Hz/pixel, and an acquisition time of 9 minutes 48 seconds.

Because the VFA technique requires correction for nonuniformities of the transmit coil sensitivity (B1), the method described by Volz et al[21] was used for B1 mapping, which compares two datasets, one acquired after full spin relaxation and one after application of a nonselective radio frequency (RF) pulse with a nominal angle of 45°. The parameters were: FOV as above, matrix = 64 x 56 x 40, TR/TE/α = 11 ms/5 ms/11°, receiver bandwidth = 260 Hz/pixel, and an acquisition time of 53 seconds.

Mapping of qT2 was performed by acquiring five turbo spin echo datasets with different TE values. The duration was 1 minute 12 seconds per dataset, i.e., 6 minutes in total. The parameters were: FOV = 240 x 180 mm^2, matrix = 192 x 144, 25 axial slices (2 mm thickness without interslice gap) covering the tumor region, TR = 4670 ms, TE = 16, 64, 96, 128 and 176 ms, receiver bandwidth = 100 Hz/pixel, acquisition of 11 spin echoes per excitation, and echo spacing of 16 ms. Mapping of qT1, B1 and qT2 were performed before GBCA administration. Mapping of qT1 and B1 were repeated, starting 5 minutes 30 seconds after standardized intravenous GBCA injection (0.05 mmol/kg gadobutrol [Gd-DO3A-butrol; Gadovist, Bayer AG, Leverkusen, Germany] followed by a 20 ml bolus of 0.9% saline).

2.3 | Postprocessing of MRI data

Tissue segmentation and data coregistration were performed with the tools FAST and FLIRT, respectively, from the FMRIB Software Library (FSL, http://www.fmrib.ox.ac.uk/fsl). Data postprocessing and analyses were performed with custom-built programs written in MatLab (MathWorks, Natick, MA). All VOIs for data analyses were selected as described below with MRIcron (http://www.mccauslandcenter.sc.edu/mricro/mricron/).

Tissue masks for white matter, gray matter and cerebrospinal fluid (which are required for correction of residual relaxation time bias in the B1 mapping data) were obtained by segmentation of the T1w dataset and applying a lower threshold of 0.999 to the resulting probability maps. B1 maps were calculated as described in the literature[21] and interpolated to attain the same matrix and voxel size as in the T1w dataset.

For qT1 mapping, the PD-weighted dataset was coregistered to the T1w dataset. Subsequently, qT1 maps were calculated pixelwise from both datasets via the VFA method.[19] Data were corrected for B1 inhomogeneities and insufficient spoiling of transverse magnetization.[22]

For qT2 mapping, the five T2w datasets acquired at different TE values were coregistered. Subsequently, qT2 maps were obtained by mono-exponential fitting of local signal intensities versus TE. The qT2 maps were only used for semiautomatic selection of the edema region.

To allow for a direct comparison and combination of the different maps obtained, qT2 maps and $qT1_{post}$ maps were coregistered to the $qT1_{pre}$ maps. As the GBCA lowered the relaxation times, the absolute qT1-difference maps were calculated as $qT1_{pre}$ - $qT1_{post}$, thus allowing a direct assessment of the CA accumulation based on qT1-difference maps (displayed with linear gray scaling). In order to obtain the relative qT1 difference in %, the absolute qT1-difference maps were divided by $qT1_{pre}$ then multiplied by 100.

To allow for calculation of absolute and relative differences of T1w images, the $T1w_{post}$ images were coregistered to the T1w images before CA ($T1w_{pre}$). As GBCA yields a shortening of T1 and thus an increase in $T1w_{post}$ image intensity, the differences were calculated as $T1w_{post}$ - $T1w_{pre}$ for the absolute difference (in arbitrary units [a.u.]) and the result was divided by $T1w_{pre}$ then multiplied by 100 to obtain the relative difference in %.

2.4 | Data analysis

Due to the heterogeneity of glioblastomas, a fully automatic selection of the various VOIs is difficult. To reduce the bias of manual VOI selection, a semiautomatic VOI selection as provided by the 3D fill tool of the MRIcron software package was used, which creates 3D VOIs on an arbitrary image dataset as follows: a seed voxel is chosen manually. The algorithm then identifies all voxels in a specified search radius that have a similar intensity to the seed voxel. The parameters that can be modified by the user are the search radius, the maximum intensity difference allowed, and the minimum intensity difference at the edges of the VOI. For each VOI, an experienced neuroradiologist (with at least 18 years of experience) selected the seed voxel manually and adapted the crucial parameters until the VOI envisaged was selected. Due to the size of the pathology, the VOIs are relatively large, thus a negligible interreader variation on results is expected, especially as the semiautomatic VOI selection was performed by an experienced neuroradiologist. For selection of the enhancing tumor VOIs, the tool was applied to the qT1-difference maps displayed with linear gray scaling, where the enhancing tumor appears hyperintense. For selection of the adjacent edema VOI, the tool was applied to the

qT2 map to select the hyperintense tumor and edema region with subsequent exclusion of all voxels belonging to the enhancing tumor VOI. The 5 mm zone VOI directly adjacent to the pathology (comprising the enhancing tumor and the edema) was determined with a custom-built program in Matlab and provided a sufficiently large VOI, which did not appear suspicious in the conventional MR images ($T1w_{post}$ and T2w). For selection of a VOI of normal appearing tissue with a diameter of between 12 and 16 mm, the seed voxel was placed on the qT2 map into an area of normal appearing tissue of the same type as the tissue at the tumor location. In general, the normal appearing tissue was selected on the contralateral hemisphere of the brain, provided this area was not affected by the tumor.

Absolute and relative GBCA-induced differences both of qT1 values and of T1w signal intensities were determined in all four VOIs (enhancing tumor, edema, 5 mm zone and normal appearing control tissue). The absolute T1w image differences were included as they are provided by most clinical scanners for visual inspection and need no further offline postprocessing; however, these values cannot be compared with other studies as they are scanner-dependent.

The analysis described above was performed for the 33 patients included in the final analysis. Neither intraobserver nor interobserver variabilities were tested. Differences between normal appearing tissue and enhancing tumor tissue, edema and the 5 mm zone, as well as between enhancing tumor and edema, and between edema and 5 mm zone, were tested with a paired Student's t-test for significance at the $P < 0.01$ level.

A visual comparison was performed between the absolute qT1-difference maps and the absolute and relative differences of T1w images to detect which modality visualized the elevated signal intensities best, thus indicating GBCA accumulation. To allow for a fair comparison of absolute qT1-difference maps and the relative and absolute differences of the T1w images, all difference maps and images were scaled to yield identical mean signal across normal appearing white matter. This was necessary due to the large range of qT1 differences in the enhancing tumor for the different patients (Table 1).

On the basis of the absolute qT1-difference maps, two neuroradiologists (both with at least 18 years of experience) and a neurologist visually assessed (on a consensus basis) the extent of CA accumulation in the edema region and the region beyond the pathology, ie, the region which appeared inconspicuous in both the conventional T1w and T2w images. The scores were 0 for no, 1 for weak, and 2 for clearly visible CA accumulation.

3 | RESULTS

Illustrative examples of glioblastomas are shown in Figures 1–4. For orientation, each figure shows (left, yellow frame) conventional clinical images: T2w with TE = 128 ms (top) and $T1w_{post}$ (bottom). In addition, the top row shows (from left to right): the T2 map used to select the edema region (A), the absolute qT1-difference map (B), and the relative (C) and absolute (D) difference of the T1w images pre- and post-CA. The bottom row shows identical images (E-H) to the top row with the VOI masks superimposed: enhancing tumor (red), edema (blue) and 5 mm zone (green). All images are shown as per neurological convention.

3.1 | Visual comparison of differences of conventional T1w images and of qT1 maps

3.1.1 | CA leakage in the edema region and necrotic center

The absolute qT1-difference maps show high values in the enhancing tumor area due to a strong accumulation of CA (Figures 1–3, B and F), but also clearly elevated qT1 differences in the edema region (Figures 1–4, B and F) as well as in the necrotic center (Figure 2, B and F), indicating local CA leakage. By contrast, the absolute differences of the T1w images fail to show CA enhancement in the edema (Figures 1–4, D and H) and necrotic region (Figure 2, D and H). The relative differences of the T1w images show a slightly elevated signal in the edema (Figures 1–4, C and G) and necrotic region (Figure 2, C and G): therefore, for visual inspection, they are better suited than the absolute T1w differences, but less informative than the absolute qT1-differences.

TABLE 1 Quantitative T1 (qT1) difference values (33 patients) for all volumes of interest (VOIs). Values are given in ms

	Enhancing tumor	Edema	5 mm zone	Normal appearing tissue
Minimum	389	-5	20	–36
Maximum	1163	319	149	94
Median	851	113	80	29
Average	838	123	81	32
Standard deviation	210	74	31	35

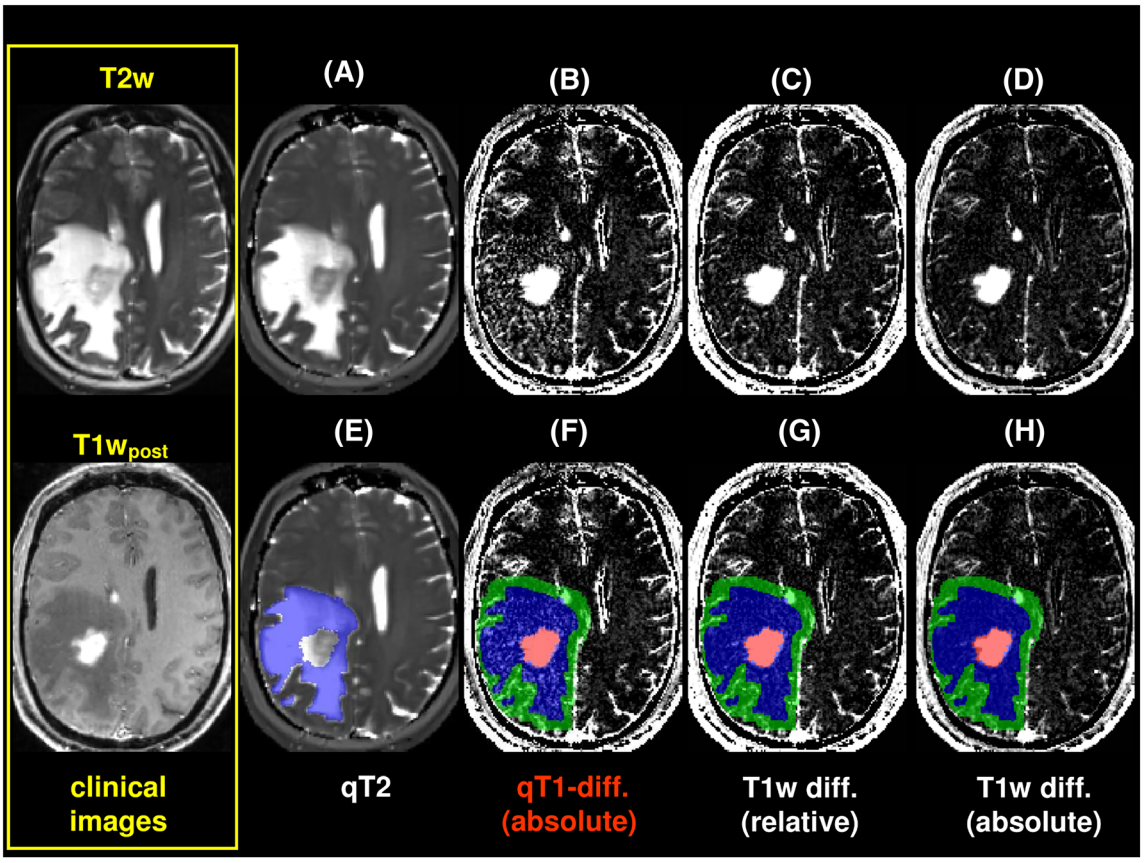

FIGURE 1 Data of a patient with a glioblastoma adjacent to the left lateral ventricle surrounded by edema and with a satellite lesion at the roof of the left lateral ventricle. The yellow frame (left) shows a conventional T2-weighted (T2w) image (top) and the T1w image post contrast agent (T1w$_{post}$) (bottom) for orientation. Further, the top and bottom rows show from left to right: quantitative T2 (qT2) map (A, E), absolute qT1-difference map (B, F) and relative (C, G) and absolute (D, H) differences of T1w images. In the bottom row, the volume of interest (VOI) masks are superimposed: enhancing tumor (red), edema (blue) and 5 mm zone (green). In contrast to the absolute difference of the T1w images (D, H), the qT1-difference map (B, F) shows elevated values in the edema region (blue mask), which is also visible but to a lower degree in the relative difference of the T1w images (C, G)

In 32 out of the 33 patients, visual assessment of the absolute qT1-difference map showed CA leakage (24 clear, eight weak) in at least a part of the edema region.

3.1.2 | CA leakage beyond the edema region

The absolute qT1-difference maps (B and F) in Figures 3 and 4 show enhancement beyond the left hemispheric edema region, which is not visible in any of the differences of T1w images (C and G, D and H). For the patient shown in Figure 4, this enhancement extends into even more superior regions.

In 21 out of the 33 patients, visual assessment of the absolute qT1-difference map showed CA leakage (10 clear, 11 weak) in areas beyond the pathology.

3.2 | Quantitative T1 values of the solid enhancing tumor, edema, 5 mm zone and normal appearing control tissue

Average values and standard deviations (n = 33) of the absolute and relative qT1 differences and the relative and absolute T1w differences for the four VOIs (enhancing tumor, edema, 5 mm zone and normal appearing tissue) are shown in Figure 5, and the respective values are provided in Table 2. The average absolute and relative qT1-difference values are highest in the enhancing tumor and are still elevated in the edema and the 5 mm zone, all values being significantly (P < 0.01) higher than the average value of normal appearing tissue. These results indicate CA leakage in

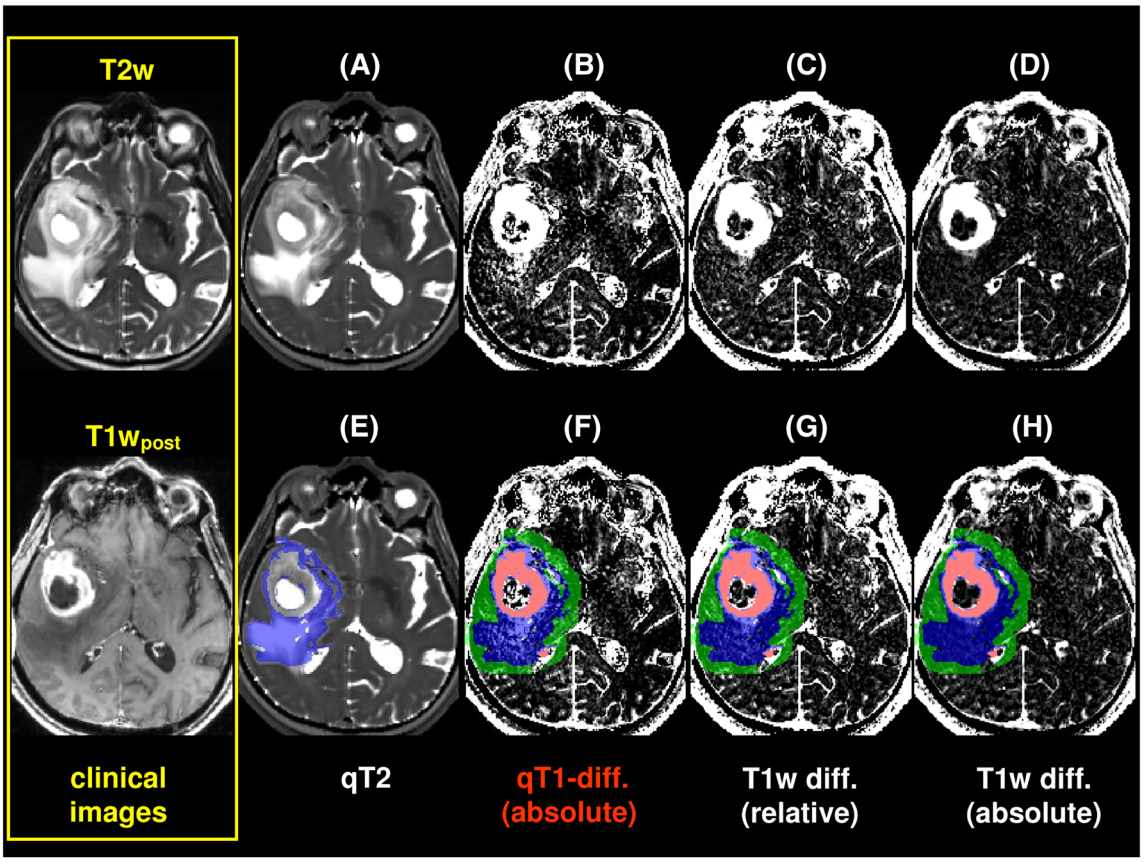

FIGURE 2 Data of a patient with a left-temporal glioblastoma with central necrosis surrounded by peritumoral edema. The yellow frame (left) shows a conventional T2-weighted (T2w) image (top) and the T1w image post contrast agent ($T1w_{post}$) (bottom) for orientation. Further, the top and bottom rows show from left to right: quantitative T2 (qT2) map (A, E), absolute qT1-difference map (B, F) and relative (C, G) and absolute (D, H) differences of T1w images. In the bottom row, the volume of interest (VOI) masks are superimposed: enhancing tumor (red), edema (blue) and 5 mm zone (green). In contrast to the absolute difference of the T1w images (D, H), the qT1-difference map (B, F) shows elevated values in the edema region (blue mask) as well as in the necrotic center, which is hardly visible in the relative difference of the T1w images (C, G) due to elevated noise

the edema region and beyond. The average difference values of T1w images (relative and absolute) show the same characteristics: compared with normal appearing tissue, they are significantly ($P < 0.01$) elevated in the enhancing part of the tumor, in the edema, and in the 5 mm zone. All results are significantly different between enhancing tumor and edema, and between edema and the 5 mm zone, at the $P < 0.01$ level, except for the absolute T1w-difference value and the relative qT1-difference value (neither of which was significantly different between the edema and the 5 mm zone).

4 | DISCUSSION

The proposed method quantifies the shortening of the T1 relaxation time due to GBCA accumulation, resulting in elevated values in the absolute qT1-difference maps ($qT1_{pre}$ - $qT1_{post}$). The considerable GBCA accumulation in the enhancing tumor results in high values in the absolute qT1-difference maps, thus easing semiautomated segmentation of the enhancing tumor mass, and also enabling determination of the enhancing lesion volume, which is particularly important for treatment planning and monitoring. This would yield a more reliable tumor size determination than the procedure according to the RANO criteria (calculating the product of the tumor extent along two orthogonal axes in 2D images of the tumor),[23] which might be inaccurate for irregular tumor shapes. An alternative volumetric method is the previously described Delta T1 method, which is based on calibrated T1w images before and after GBCA administration and thus does not require qT1 maps.[24,25] Conventional T1w images and their absolute and relative difference images pre- and post-CA administration show the enhancing part of the tumor as well. By contrast, the moderate CA accumulation in the edema region, and in some cases even beyond, is only visible in the absolute qT1-difference maps, whereas the absolute difference images ($T1w_{post}$ - $T1w_{pre}$) of the conventional T1w images fail to show this effect. The relative difference of the T1w images shows this effect in a few cases, but to a much lesser extent, when compared with the absolute qT1-difference maps.

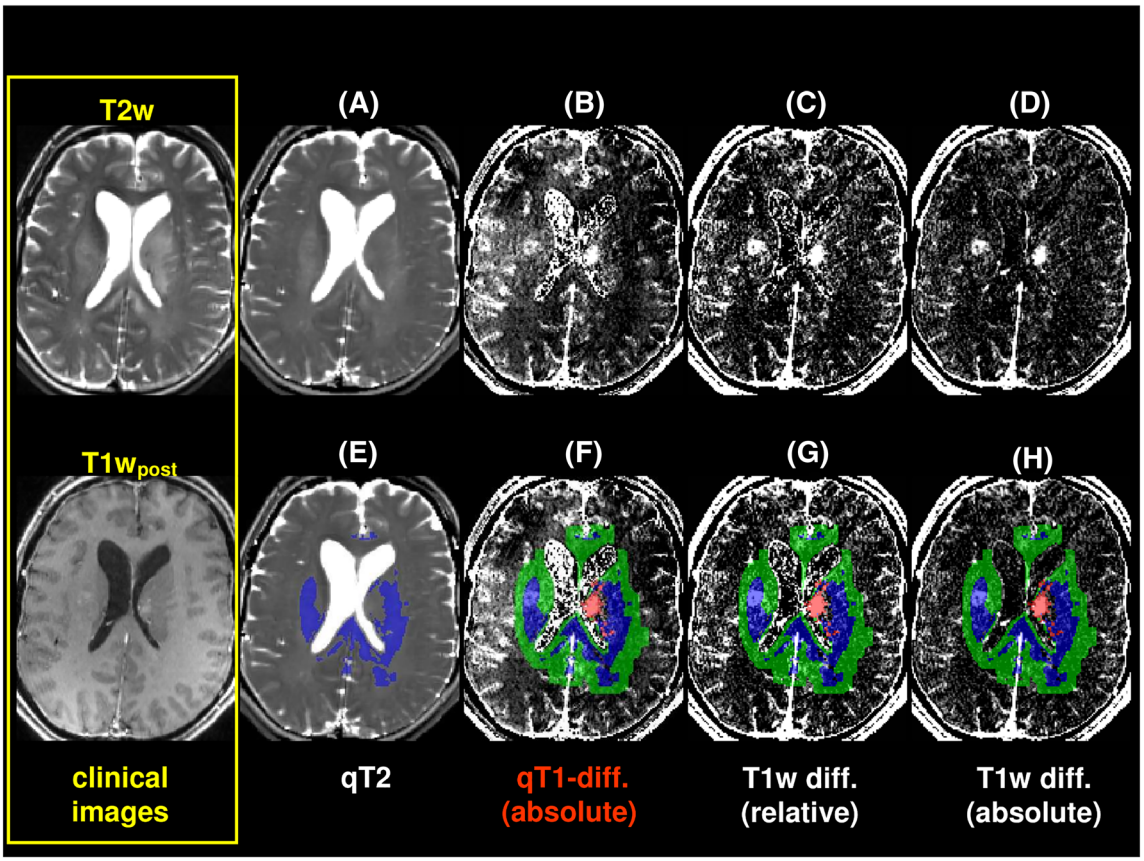

FIGURE 3 Data of a patient with a glioblastoma adjacent to the right lateral ventricle and surrounded by edema. The yellow frame (left) shows a conventional T2-weighted (T2w) image (top) and the T1w image post contrast agent ($T1w_{post}$) (bottom) for orientation. Further, the top and bottom rows show from left to right: quantitative T2 (qT2) map (A, E), absolute qT1-difference map (B, F) and relative (C, G) and absolute (D, H) differences of T1w images. In the bottom row, the volume of interest (VOI) masks are superimposed: enhancing tumor (red), edema (blue) and 5 mm zone (green). The qT1-difference map (B, F) shows enhancement beyond the left-sided edema region (blue mask) and 5 mm zone (green mask), which is not visible in the T1w difference images (C, D, G, H)

The moderate GBCA accumulation beyond the enhancing tumor is only consistently visible in the absolute qT1-difference maps, being manifest in at least parts of the edema region (97% of patients) and in many cases even beyond (64%). A recent study analyzing the peritumoral edema in malignant gliomas also reports a heterogeneous pattern of qT1 values in this region after GBCA administration.[26] This moderate GBCA accumulation might indicate angiogenically active glioma cell infiltration into these regions, i.e., into areas that do not appear suspicious in conventional T1w MRI. Although this "angiogenic switch" is a hallmark of high-grade gliomas,[27] the angiogenic potency might be heterogeneous, and thus differ between different tumor areas. This heterogeneity might explain why the intensity and extent of the subtle enhancement beyond the enhancing tumor (as observed in the absolute qT1-difference maps) differed considerably between the glioblastomas. Therefore, the absolute qT1-difference maps, in contrast to conventional T1w images and their differences, appear to be able to visualize the infiltration areas, which would allow their inclusion in therapy.

The finding of elevated absolute qT1-difference values in the edema region stands in line with the results of several previous MRI and MRS studies that also show changes for different MR parameters beyond the enhancing part of glioblastomas: a stripe-like pattern of regional CBV increase was found in a defined region adjacent to the contrast-enhancing tumor, which then transformed into enhancing tumor tissue in the follow-up[16]; the VOI analysis of BOLD-based relative oxygen extraction fraction (rOEF) maps revealed potentially hypoxic tumor regions with high rOEF in the nonenhancing infiltration zone[28]; peritumoral fiber structures showed significant decreases of N-acetyl-aspartate concentrations and fiber densities when compared with the contralateral side.[29] Further studies based on a combination of dynamic contrast enhanced (DCE) and dynamic susceptibility contrast (DSC) MRI[30] or using machine-learning algorithms on a set of different MRI modalities[31] suggest that these techniques are promising candidates for distinguishing between vasogenic edema and tumor-containing edema, which appear similar in conventional MRI. The method presented here reveals a new biological aspect of peritumoral alterations in glioblastomas and may thus help with this differentiation, which is important for therapy response assessment.

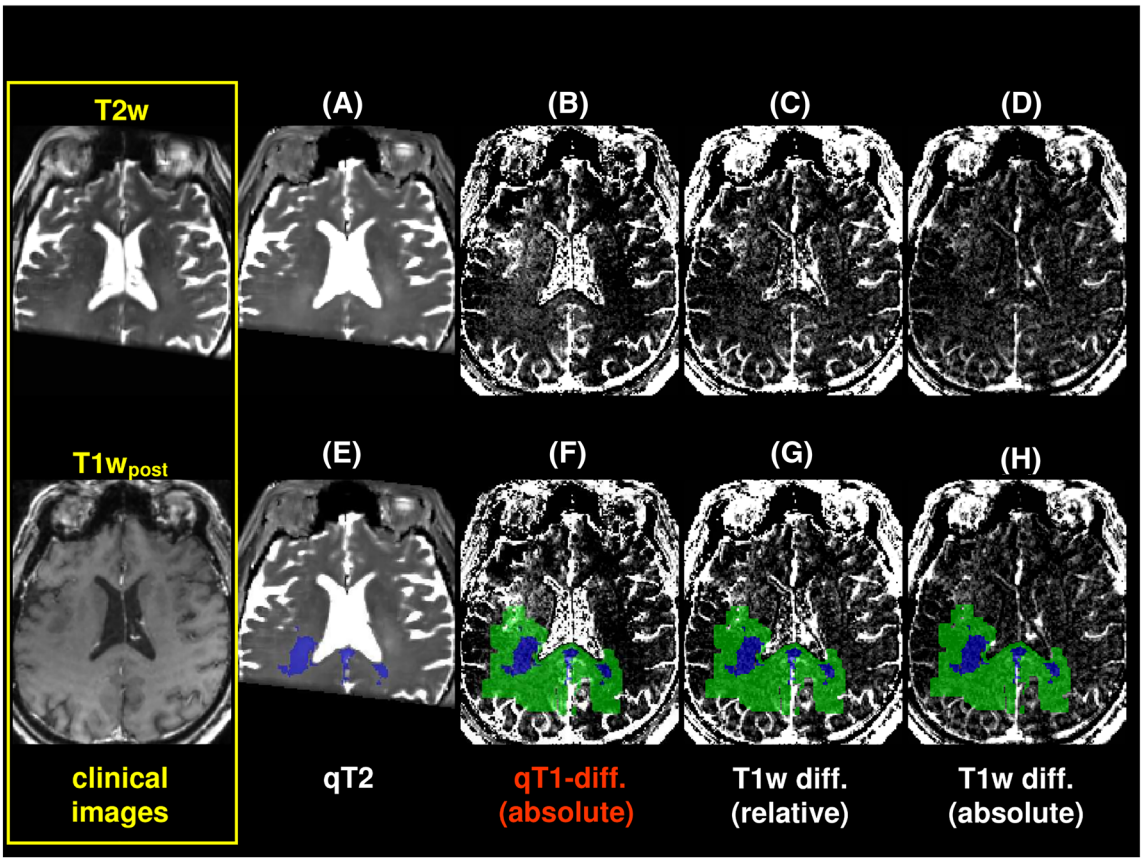

FIGURE 4 Data of a patient with a left-temporal glioblastoma surrounded by edema; the slice shown depicts the most superior part of the edema region. The yellow frame (left) shows a conventional T2-weighted (T2w) image (top) and the T1w image post contrast agent ($T1w_{post}$) (bottom) for orientation. Further, the top and bottom rows show from left to right: quantitative T2 (qT2) map (A, E), absolute qT1-difference map (B, F) and relative (C, G) and absolute (D, H) differences of T1w images. In the bottom row, the volume of interest (VOI) masks are superimposed: edema (blue) and 5 mm zone (green). The qT1-difference map (B, F) shows enhancement in the left hemisphere beyond the edema region (blue mask) and 5 mm zone (green mask), which is not visible in the T1w difference images (C, D, G, H)

Moderate GBCA accumulation beyond the enhancing tumor might also be the result of Gd molecules diffusing from the enhancing tumor into the edema and the 5 mm zone. However, considering the large size of the Gd-chelate complexes and the short time window between GBCA application and data acquisition, such a rapid diffusion appears rather unlikely.

In this context, it would also be of interest to investigate the signal time course in the absolute qT1-difference maps over the first few hours after GBCA administration by acquiring $qT1_{post}$ maps at different postinjection time points. This might show stronger contrast enhancement due to an increased time window for GBCA accumulation.

Alternatively, cytokines from the solid tumor area might diffuse into the peritumoral zone, inducing gene expression of vascular endothelial growth factor (VEGF), which causes peripheral BBB leakage, allowing water and CA molecules to pass through the vessel walls. However, the question arises whether a direct diffusion of cytokines or other proangiogenic factors across relatively large distances from the enhancing tumor is likely.[32] A more conceivable explanation would be the expression of cytokines by tumor cells that have spread over the brain area, impairing the vessels in their vicinity. The effect of VEGF on vessel permeability may induce an edema which extends beyond the infiltration areas of a tumor. This effect, which is also known about from VEGF-producing noninfiltrating meningiomas, may partly be explained by water diffusion. Taking all of this into account, the T1 reduction due to CA leakage (which is limited to the area of VEGF-expressing glioma cells) may be more specific to detect tumor infiltration[33] than the T2 prolongation due to water leakage, since the latter is also increased in gliosis, inflammation and necrosis.

A recent postsurgery study in 18 glioblastoma patients investigated relative T1-shortening induced by intravenous GBCA administration in 6-week intervals during radiochemotherapy.[34] The qT1-difference maps showed a cloudy enhancement at the margin of the residual tumor that was not visible in conventional MRI. Interestingly, patients with an early and marked decrease of the cloudy enhancement under therapy had a longer progression-free survival.[34] This supports the "infiltration hypothesis", since the better prognosis indicates that tumor cells in the infiltration zone have responded well to therapy.

Furthermore, the question arises why the conventional T1w images and their differences in most cases failed to show an effect in the edema region, although the local T1 reduction post-CA should yield a distinct signal increase in the $T1w_{post}$ images. The problem is that conventional

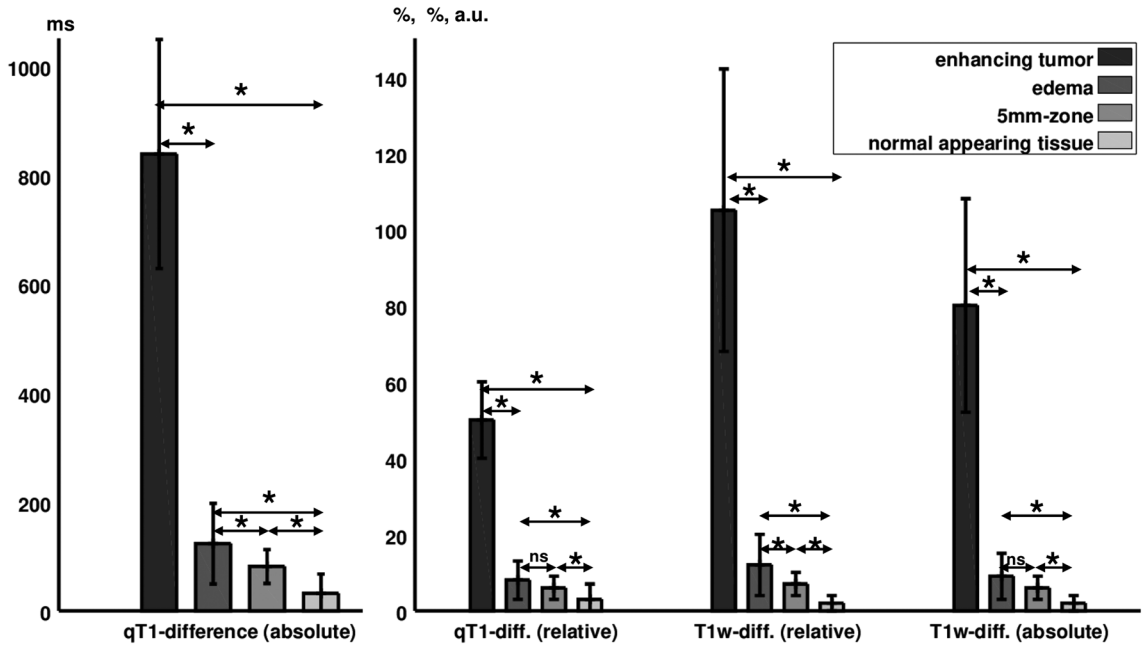

FIGURE 5 Average values and standard deviations (n = 33) of the absolute and relative quantitative T1 (qT1) differences, and the relative and absolute differences of the T1-weighted (T1w) images for all volumes of interest (VOIs) (enhancing tumor, edema, 5 mm zone and normal appearing tissue). Values between the VOIs differ significantly at the $P < 0.01$ level when indicated with * above the arrows. Only the values between edema and 5 mm zone for the relative qT1-difference and the absolute T1w difference were not significant (indicated with "ns" above the arrows)

TABLE 2 Absolute and relative differences of quantitative T1 (qT1) values and of signal intensities in the T1-weighted (T1w) images for all volumes of interest (VOIs). The mean values ± standard deviations (33 patients) are reported

	Enhancing tumor	Edema	5 mm zone	Normal appearing tissue
qT1-diff. (absolute), ms	838 ± 210	123 ± 74	81 ± 31	32 ± 35
qT1-diff. (relative), %	50 ± 10	8 ± 5	6 ± 3	3 ± 4
T1w-diff. (relative), %	105 ± 37	12 ± 8	7 ± 3	2 ± 2
T1w-diff. (absolute), a.u.	80 ± 28	9 ± 6	6 ± 3	2 ± 2

weighted data always show mixed contrasts. In the particular case of T1w data, image intensities are not only influenced by local T1 values but are also proportional to the local equilibrium magnetization (M0) that depends on several parameters: the local T2* value (due to the use of a gradient echo technique with a nonzero TE) and inhomogeneities of the sensitivity profiles of the RF coils used for signal transmission and reception. Given the paramagnetic properties of GBCAs, they will lower T2*, and thus reduce M0. The resulting decrease in signal intensity may partly mask the effect of interest, i.e., the signal increase arising from T1 reduction. A more detailed analysis of the data acquired for this study showed that the T1 reduction itself would yield a signal increase in the T1w images by ~ 10% in the edema region, but that this effect is accompanied by an M0 reduction of ~ 4% in this region, thus reducing the effect of interest. This could explain why there is a minor effect in the relative difference of T1w images pre- and post-CA administration. Furthermore, due to interscan subject motion, head positions may be different for the scans performed before and after CA administration, even if the subject remains still during each scan so that single datasets are free from motion artifacts. Although this effect is accounted for by means of data coregistration, a change of the head position relative to the RF coils yields different sensitivity nonuniformity profiles across the head and thus a different bias in the spatial M0 distribution. Again, the resulting signal nonuniformity may easily mask the effect of interest. By contrast, the qT1 maps supply pure contrasts, i.e., the signal intensity depends exclusively on the local T1 value and is not influenced by changes in T2* or the relative RF coil bias. As the calculation of the qT1 maps is based on the quotient of a PD-weighted and a T1w dataset, any bias induced by M0 (and therefore T2*), or by the receive RF coil sensitivity profile, is eliminated. Furthermore, the transmit RF coil bias is measured separately before and after CA administration and is accounted for in each case, as was explained earlier in the Materials and Methods section.

The current study has some limitations: (i) a histopathological confirmation of tumor infiltration beyond the enhancing part of the tumor and beyond the areas of prolonged T2 was not performed, as the resection of brain tissue which was not suspicious in conventional MRI would not be justifiable ethically. However, recent preclinical studies show that glioma cell infiltration reaches beyond the area of signal hyperintensity in

T2w images[35,36]; (ii) to reduce the scanning time, T2 mapping was restricted to 25 slices covering a slab of 5 cm. Therefore, in some patients, the edema region was not completely covered, which may have changed quantitative values for the edema region slightly; and (iii) it should also be noted that CA accumulation remains only an indirect sign of potential glioma cell infiltration. Thus, the possibility cannot be excluded that qT1 mapping may miss some tumor areas. However, given that the angiogenic switch is a hallmark of malignancy in gliomas, this method appears to be suitable to detect the infiltration zones.

A combination of the presented method with qMRI techniques measuring further parameters (DTI, CBV, T2, PD, perfusion) and more novel MRI techniques (diffusion kurtosis imaging, chemical exchange saturation transfer) might provide a more precise characterization of the area beyond the enhancing tumor and emerge as a useful tool for initial tumor characterization and for treatment monitoring.[37]

In conclusion, in patients with untreated glioblastomas, the qMRI method presented here clearly delineates CA leakage beyond the enhancing tumor areas, i.e., in the edema region and even beyond, indicating a deficient BBB, and therefore most likely infiltration with tumor cells. By contrast, for conventional T1w images, relative difference images delineated areas of CA leakage beyond the enhancing tumor areas in only a few cases and relatively weakly, whereas absolute difference images consistently failed to show this effect at all. Future studies could evaluate whether the magnitude of CA accumulation, for which the method proposed here provides a quantitative parameter by means of relaxometry, allows graduating different infiltration zones. If so then the extent of CA accumulation may help to improve treatment planning.

ABBREVIATIONS

Abbreviations used: a.u., arbitrary units; B1, transmit coil sensitivity; BBB, blood–brain barrier; CA, contrast agent; CBV, cerebral blood volume; DTI, diffusion tensor imaging; Gd, gadolinium; GBCA, gadolinium-based contrast agent; M0, equilibrium magnetization; MRSI, MR spectroscopic imaging; PD, proton density; PET, positron emission tomography; qT1, quantitative T1; $qT1_{pre}$, quantitative T1 before intravenous CA administration; $qT1_{post}$, quantitative T1 after intravenous CA administration; RF, radio frequency; rOEF, relative oxygen extraction fraction; T1w, T1-weighted; T2w, T2-weighted; $T1w_{pre}$, T1w image before CA; $T1w_{post}$, T1w image post-CA; VEGF, vascular endothelial growth factor; VFA, variable flip angle; VOI, volume of interest.

ORCID

Ulrike Nöth https://orcid.org/0000-0003-0699-4088

REFERENCES

1. Louis DN, Ohgaki H, Wiestler OD, et al. The 2007 WHO classification of tumours of the central nervous system. *Acta Neuropathol*. 2007;114:97-109.
2. Stummer W, Reulen H-J, Meinel T, et al. Extent of resection and survival in glioblastoma multiforme: identification of and adjustment for bias. *Neurosurgery*. 2008;62:564-574.
3. Ahmadipour Y, Kaur M, Pierscianek D, et al. Association of surgical resection, disability, and survival in patients with glioblastoma. *J Neurol Surg A: Cent Eur Neurosurg*. 2019;80:262-268.
4. Haj A, Doenitz C, Schebesch K-M, et al. Extent of resection in newly diagnosed glioblastoma: impact of a specialized neuro-oncology care center. *Brain Sci*. 2018;8(5):1-10.
5. Tang S, Liao J, Long Y. Comparative assessment of the efficacy of gross total versus subtotal total resection in patients with glioma: a meta-analysis. *Int J Surg*. 2019;63:90-97.
6. Watanabe M, Tanaka R, Takeda N. Magnetic resonance imaging and histopathology of cerebral gliomas. *Neuroradiology*. 1992;34:463-469.
7. Kelly PJ, Daumas-Duport C, Kispert DB, Kall BA, Scheithauer BW, Illig JJ. Imaging-based stereotaxic serial biopsies in untreated intracranial glial neoplasms. *J Neurosurg*. 1987;66:865-874.
8. Earnest F, Kelly PJ, Scheithauer BW, et al. Cerebral astrocytomas: histopathologic correlation of MR and CT contrast enhancement with stereotactic biopsy. *Radiology*. 1988;166:823-827.
9. McKnight TR, von dem Bussche MH, Vigneron DB, et al. Histopathological validation of a three-dimensional magnetic resonance spectroscopy index as a predictor of tumor presence. *J Neurosurg*. 2002;97:794-802.
10. Sternberg EJ, Lipton ML, Burns J. Utility of diffusion tensor imaging in evaluation of the peritumoral region in patients with primary and metastatic brain tumors. *Am J Neuroradiol*. 2014;35:439-444.
11. Pirotte B, Goldman S, Dewitte O, et al. Integrated positron emission tomography and magnetic resonance imaging-guided resection of brain tumors: a report of 103 consecutive procedures. *J Neurosurg*. 2006;104:238-253.
12. Rieken S, Habermehl D, Giesel FL, et al. Analysis of FET-PET imaging for target volume definition in patients with gliomas treated with conformal radiotherapy. *Radiother Oncol*. 2013;109:487-492.
13. Price SJ, Jena R, Burnet NG, et al. Improved delineation of glioma margins and regions of infiltration with the use of diffusion tensor imaging: an image-guided biopsy study. *Am J Neuroradiol*. 2006;27:1969-1974.
14. Aronen HJ, Gazit IE, Louis DN, et al. Cerebral blood volume maps of gliomas: comparison with tumor grade and histologic findings. *Radiology*. 1994;191:41-51.
15. Sugahara T, Korogi Y, Kochi M, et al. Correlation of MR imaging-determined cerebral blood volume maps with histologic and angiographic determination of vascularity of gliomas. *Am J Roentgenol*. 1998;171:1479-1486.
16. Blasel S, Franz K, Ackermann H, Weidauer S, Zanella F, Hattingen E. Stripe-like increase of rCBV beyond the visible border of glioblastomas: site of tumor infiltration growing after neurosurgery. *J Neurooncol*. 2011;103:575-584.

17. Plate KH, Breier G, Weich HA, Mennel HD, Risau W. Vascular endothelial growth factor and glioma angiogenesis: coordinate induction of VEGF receptors, distribution of VEGF protein and possible in vivo regulatory mechanisms. *Int J Cancer*. 1994;59:520-529.
18. Plate KH, Mennel HD. Vascular morphology and angiogenesis in glial tumors. *Exp Toxicol Pathol*. 1995;47:89-94.
19. Venkatesan R, Lin W, Haacke EM. Accurate determination of spin-density and T1 in the presence of RF-field inhomogeneities and flip-angle miscalibration. *Magn Reson Med*. 1998;40:592-602.
20. Preibisch C, Deichmann R. T1 mapping using spoiled FLASH-EPI hybrid sequences and varying flip angles. *Magn Reson Med*. 2009;62:240-246.
21. Volz S, Nöth U, Rotarska-Jagiela A, Deichmann R. A fast B1-mapping method for the correction and normalization of magnetization transfer ratio maps at 3 T. *Neuroimage*. 2010;49:3015-3026.
22. Preibisch C, Deichmann R. Influence of RF spoiling on the stability and accuracy of T1 mapping based on spoiled FLASH with varying flip angles. *Magn Reson Med*. 2009;61:125-135.
23. Wen PY, Macdonald DR, Reardon DA, et al. Updated response assessment criteria for high-grade gliomas: response assessment in neuro-oncology working group. *J Clin Oncol*. 2010;28:1963-1972.
24. Bedekar D, Jensen T, Rand S, Malkin M, Connelly J, Schmainda K. Delta T1 method: an automatic post-contrast ROI selection technique for brain tumors 18th Meeting of the ISMRM, Stockholm, Sweden 2010. *Proc. Intl. Soc. Mag. Reson. Med*. 2010;18:2175.
25. Schmainda K, Prah M, Hu LS, et al. Moving toward a consensus DSC-MRI protocol: validation of a low-flip angle single-dose option as a reference standard for brain tumors. *Am J Neuroradiol*. 2019;40:626-633.
26. Blystad I, Warntjes JBM, Smedby Ö, Lundberg P, Larsson EM, Tisel A. Quantitative MRI for analysis of peritumoral edema in malignant gliomas. *PLoS ONE*. 2017;12:e0177135.
27. Hanahan D, Folkman J. Patterns and emerging mechanisms of the angiogenic switch during tumorigenesis. *Cell*. 1996;86:353-364.
28. Tóth V, Förschler A, Hirsch NM, et al. MR-based hypoxia measures in human glioma. *J Neurooncol*. 2013;115:197-207.
29. Stadlbauer A, Hammen T, Buchfelder M, et al. Differences in metabolism of fiber tract alterations in gliomas: a combined fiber density mapping and magnetic resonance spectroscopic imaging study. *Neurosurgery*. 2012;71:454-463.
30. Artzi M, Blumenthal DT, Bokstein F, et al. Classification of tumor area using combined DCE and DSC MRI in patients with glioblastoma. *J Neurooncol*. 2015;121:349-357.
31. Artzi M, Liberman G, Blumenthal DT, Aizenstein O, Bokstein F, Ben Bashat D. Differentiation between vasogenic edema and infiltrative tumor in patients with high-grade gliomas using texture patch-based analysis. *J Magn Reson Imaging*. 2018;48:729-736.
32. Kihara T, Ito J, Miyake J. Measurement of biomolecular diffusion in extracellular matrix condensed by fibroblasts using fluorescence correlation spectroscopy. *PLoS ONE*. 2013;8:e82382.
33. Lescher S, Jurcoane A, Veit A, Bähr O, Deichmann R, Hattingen E. Quantitative T1 and T2 mapping in recurrent glioblastomas under bevacizumab: earlier detection of tumor progression compared to conventional MRI. *Neuroradiology*. 2015;57:11-20.
34. Müller A, Jurcoane A, Kebir S, et al. Quantitative T1-mapping detects cloudy-enhancing tumor compartments predicting outcome of patients with glioblastoma. *Cancer Med*. 2017;6:89-99.
35. Breckwoldt MO, Bode J, Sahm F, et al. Correlated MRI and ultramicroscopy (MR-UM) of brain tumors reveals vast heterogeneity of tumor infiltration and neoangiogenesis in preclinical models and human disease. *Front Neurosci*. 2019;12:1004.
36. Vallatos A, Al-Mubarak HFI, Birch JL, et al. Quantitative histopathologic assessment of perfusion MRI as a marker of glioblastoma cell infiltration in and beyond the peritumoral edema region. *J Magn Reson Imaging*. 2019;50:529-540.
37. Hyare H, Thust S, Rees J. Advanced MRI techniques in the monitoring of treatment of gliomas. *Curr Treat Options Neurol*. 2017;19:11.

How to cite this article: Nöth U, Tichy J, Tritt S, Bähr O, Deichmann R, Hattingen E. Quantitative T1 mapping indicates tumor infiltration beyond the enhancing part of glioblastomas. *NMR in Biomedicine*. 2020;33:e4242. https://doi.org/10.1002/nbm.4242